Leader-laggard synchronization of polarization chaos in mutually coupled free-running VCSELs

Zhang, Xiaomai; Li, Pu; Jia, Zhiwei; Shore, K. Alan; Wang, Yuncai

Opt. Express

[Cyswllt i'r cyhoeddiad / Link to publication](#)

Leader-laggard synchronization of polarization chaos in mutually coupled free-running VCSELs

Xiaomai Zhang,[1] Pu Li,[1,2,*] Zhiwei Jia,[1] K. Alan Shore,[3] and Yuncai Wang[2]

[1]*Key Laboratory of Advanced Transducers and Intelligent Control System, Ministry of Education, Taiyuan University of Technology, Taiyuan 030024, China*

[2]*Guangdong Provincial Key Laboratory of Photonics Information Technology, School of Information Engineering, Guangdong University of Technology, Guangzhou 510006, China*

[3]*School of Computer Science and Electronic Engineering, Bangor University, Wales LL57 1UT, UK*

*lipu8603@126.com

Abstract: We systematically study the leader-laggard synchronization of polarization chaos in mutually coupled free-running vertical cavity surface emitting semiconductor lasers in two cases of parallel and orthogonal injection. Specifically, we quantitatively investigate the effect of critical external parameter mismatch such as the coupling intensity and frequency detuning on the leader-laggard relationship utilizing the cross-correlation function. When the difference between two main cross-correlation peak values exceeds 0.1, the leader-laggard relationship can be viewed to be stable. Our results demonstrate that compared with the coupling strength, the frequency detuning is the dominant factor in determining the stability of the leader-laggard relationship. The exchange of the leader-laggard role occurs within a frequency detuning region from -5 GHz to 5 GHz for both parallel and orthogonal injection. Once the leader-laggard relationship is stable, the difference between the two cross-correlation values can reach 0.242 for negative frequency detuning, but the corresponding value is only 0.146 under positive frequency detuning.

1. Introduction

Laser chaos synchronization has been a hot topic since the pioneering work of Colet and Roy [1–3], which has been widely applied in many fields such as public channel encryption [4–6] and secure key distribution [7–9]. Coupling semiconductor lasers are often used for observing a variety of chaotic synchronization phenomena [10–12].

Because a propagation time delay is inevitable in coupled systems, one laser usually oscillates in advance of the other by a time period equal to the delay time [13,14]. This phenomenon is called leader-laggard chaos synchronization (LLCS) [15–17]. Until now, there have been many associated reports on this kind of LLCS in semiconductor lasers [18–22]. Typically, Ozaki *et al*. theoretically analyzed the leader-laggard relationship in an open-loop configuration by using vertical cavity surface emitting semiconductor lasers (VCSELs) subject to individual self-feedback [18]. Jiang *et al*. numerically investigated the properties of LLCS in closed-loop configuration of two mutually coupled external-cavity semiconductor lasers [19]. Kanno *et al*. experimentally found that the leader-laggard relation can spontaneously be exchanged in a closed-loop system [20]. Nevertheless, the semiconductor lasers used in the above-mentioned systems commonly require an external perturbation such as optical feedback to be driven into chaos [23–25]. In consequence, a weak periodicity is imposed in the chaotic outputs [26], and thus degrades the communication security of these LLCS systems [27].

Polarization chaos, a new kind of optical chaos, has been demonstrated in recent years that it can be directly generated in a free-running VCSEL with no additional external perturbation [28]. This simple structure not only meets the current needs of photonic integration, but also enables the elimination of the weak periodicity in chaotic sources [29]. Interest in polarization

chaos has led to some explorations on its associated synchronization characteristics in recent years. For instance, Virte *et al*. observed the synchronization of polarization chaos in zero-delay unidirectional coupling free-running VCSELs [30]. Our group also demonstrated polarized chaos synchronization in a zero-delay mutual coupling free-running VCSELs [31]. However, it must be pointed out that the existing reports on polarization chaos synchronization do not consider the coupling time delay. That is, there is a lack of a thorough understanding on time-delay induced the LLCS of polarization chaos.

In this paper, we systematically investigate the LLCS in mutually coupled free-running chaotic VCSELs with non-zero propagation time delay. To be specific, we consider two scenarios: one is parallel injection and the other is orthogonal injection. Through using the cross-correlation function, we quantitatively analyze the effect of coupling intensity k_{inj} and frequency detuning Δf on the leader-laggard relationship. When the difference value between two main cross-correlation peaks is above 0.1, the leader-laggard relationship can be regarded to be stable. Our simulation results show that the frequency detuning Δf is the dominant factor affecting the leader-lagged relationship over and above the injection strength. The leader-laggard role is exchanged at the frequency detuning range of -5 GHz $< \Delta f <$ 5 GHz in both parallel and orthogonal injection due to the propagation time delay. On the other hand, when the leader-laggard relationship is located in the stable regions of -10 GHz $< \Delta f <$ -5 GHz or 10 GHz $> \Delta f >$ 5 GHz, for the case of negative frequency detuning, the difference of cross-correlation can reach 0.242, but the corresponding value is only 0.146 in the case of positive frequency detuning.

2. Theoretical model

Figure 1 depicts the schematic for the LLCS of mutually coupled free-running VCSELs with time delay in parallel or orthogonal injection scenarios. Both VCSELs (VCSEL1 and VCSEL2) without additional external perturbation directly operate in a chaotic regime with two coexisting polarizations: X polarization (XP) and Y polarization (YP). The output of VCSEL1 injects into VCSEL2 after passing through a beam splitter (BS1), a half-wave plate (HWP1), an optical isolator (ISO1) and a neutral density filter (NDF1). The output of VCSEL2 experiences a similar process to form a mutually coupled structure. Note, the HWPs (HWP1, HWP2) are inserted into their own optical path to match the polarization directions between the two VCSELs for achieving parallel injection (i.e. the XP and YP light of VCSEL1 enter the VCSEL2 along their own same polarization directions) or orthogonal injection (i.e. the XP and YP light from VCSEL1 is injected perpendicularly to the YP and XP directions of the VCSEL2). The ISOs (ISO1, ISO2) are used to ensure unidirectional transmission, while the NDFs (NDF1, NDF2) are employed to independently control the injection strength of their own path, respectively. In this way, the coupling time delays in two injection scenarios can be ensured to be identical, but the injection strength from VCSEL1 to VCSEL2 can be different with that from VCSEL2 to VCSEL1.

The free-running VCSEL can be simulated based on the well-known spin flip model (SFM) with noise terms [32–34]. Considering the influence of mutually injected fields, we can extend the SFM describing the slow-varying electric field complex amplitude (E), the total number of inversion carriers (N), and the spin flipping difference in carrier number (n) as follows:

$$\frac{dE_x^{1,2}}{dt} = \kappa^{1,2}\left(1 + i\alpha^{1,2}\right)\left[\left(N^{1,2} - 1\right)E_x^{1,2} + in^{1,2}E_y^{1,2}\right] - \left(\gamma_\alpha^{1,2} + i\gamma_p^{1,2}\right)E_x^{1,2}$$
$$+ k_{inj_x}^{21,12}E_x^{2,1}\left(t - \tau_c\right)e^{-i\omega_0^{2,1}\tau_c} \mp i\Delta\omega E_x^{1,2} + F_x^{1,2} \tag{1}$$

$$\frac{dE_y^{1,2}}{dt} = \kappa^{1,2}(1 + i\alpha^{1,2})[(N^{1,2} - 1)E_y^{1,2} - in^{1,2}E_x^{1,2}] + (\gamma_\alpha^{1,2} + i\gamma_p^{1,2})E_y^{1,2}$$
$$+ k_{inj_y}^{21,12}E_y^{2,1}(t - \tau_c)e^{-i\omega_0^{2,1}\tau_c} \mp i\Delta\omega E_y^{1,2} + F_y^{1,2} \tag{2}$$
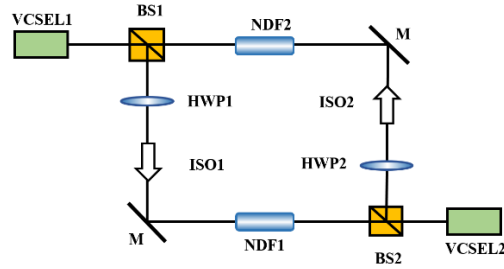
Fig. 1. Schematic for polarization chaos synchronization in two mutually coupled VCSELs in two cases of parallel optical injection and orthogonal optical injection. BS1, BS2: beam splitters; HWP1, HWP2: half-wave plates; ISO1, ISO2: optical isolators; NDF1, NDF2: neutral density filters; M1, M2: mirrors.

$$\frac{dN^{1,2}}{dt} = -\gamma_N^{1,2}[N^{1,2}(1 + |E_x^{1,2}|^2 + |E_y^{1,2}|^2) - \mu^{1,2}]$$
$$-\gamma_N^{1,2}[in^{1,2}(E_y^{1,2}E_x^{*1,2} - E_x^{1,2}E_y^{*1,2})] \tag{3}$$

$$\frac{dn^{1,2}}{dt} = -\gamma_s^{1,2}n^{1,2} - \gamma_N^{1,2}[n^{1,2}(|E_x^{1,2}|^2 + |E_y^{1,2}|^2)]$$
$$-\gamma_N^{1,2}[iN^{1,2}(E_y^{1,2}E_x^{*1,2} - E_x^{1,2}E_y^{*1,2})] \tag{4}$$

In these equations, the superscripts 1 and 2 signify VCSEL1 and VCSEL2, while the subscripts x and y represent the XP and YP modes, respectively. F_x and F_y stand for the noise terms arising from spontaneous emission. Equations (1) and (2) represent the expressions of the change in the XP and YP fields during parallel injection. For the case of orthogonal injection, $k_{\text{inj x}}$ and E_x in the second line of Eq. (1) should be replaced into $k_{\text{inj y}}$ and E_y, while $k_{\text{inj y}}$ and E_y in the second line of Eq. (2) should be replaced into $k_{\text{inj x}}$ and E_x. $k_{\text{inj}} = r_{inj}/\tau_{in}$ is the injection rate, where r_{inj} is the injection strength and τ_{in} is the round-trip time of the laser internal cavity. $\omega_0 = (\omega_1 + \omega_2)/2$ is the average angular frequency of the system, where ω_1 and ω_2 are the angular frequencies of VCSEL1 and VCSEL2, respectively. $\Delta\omega = (\omega_2 - \omega_1)/2$ is the angular frequency detuning. The other parameters and their values in the simulation see Table 1 [29]. In particular, we point that the spin flip relaxation rate γ_s strongly depends on growth conditions or manufacture of the VCSEL and its value can range from a few tens of ns^{-1} to a few thousands of ns^{-1} [32,35].

Table 1. VCSEL Parameters and their values used in simulation

Parameter	Symbol	Value
Field decay rate	κ	600 ns^{-1}
Linewidth enhancement factor	α	3
Carrier decay rate	γ_N	1 ns^{-1}
Spin-flip relaxation rate	γ_S	20 ns^{-1}
Linear dichroism	γ_a	-0.7 ns^{-1}
Linear birefringence	γ_p	25 ns^{-1}
Injection rate from VCSEL1 to VCSEL2	$k_{\text{inj}}^{1,2}$	100 ns^{-1}
Injection rate from VCSEL2 to VCSEL1	$k_{\text{inj}}^{2,1}$	50 ~150 ns^{-1}
Propagation time delay	τ	3×10^{-9} s
Injection current (I_{th})	μ	1~3
Wavelength	λ	980 nm

In the following Section, we will investigate the LLCS of mutually coupled free-running VCSELs with time delay in detail. Specifically, we analyze the effect of injection rate difference $\Delta k_{\text{inj}} = k_{\text{inj}}^{1,2} - k_{\text{inj}}^{2,1}$ and frequency detuning $\Delta f = \Delta \omega / 2\pi$ on the stability of the LLCS. Before that, we here introduce two cross-correlation coefficients (C_1 and C_2) on the intensity timeseries of the VCSEL1 and VCSEL2, because they are critical parameters that can quantitatively characterize the leader-laggard relationship. As shown in Eqs. (5) and (6), C_1 and C_2 are defined as below:

$$C_1(t) = \frac{\left\langle [I_1(t - \tau) - \bar{I}_1][I_2(t) - \bar{I}_2] \right\rangle}{\sigma_1 \sigma_2} \tag{5}$$

$$C_2(t) = \frac{\left\langle [I_1(t) - \bar{I}_1][I_2(t - \tau) - \bar{I}_2] \right\rangle}{\sigma_1 \sigma_2}, \tag{6}$$

where $I_1(t) = |E_1(t)|^2$ and $I_2(t) = |E_2(t)|^2$ indicate the intensity timeseries of the VCSEL1 and VCSEL2, respectively. 'I_1 is the intensity mean value of VCSEL1 while 'I_2 is the intensity mean value of VCSEL2. ‹·› denotes an operator of the time averaging. σ_1 and σ_2 are the standard deviation of the intensity timeseries of VCSEL1 and VCSEL2, respectively. It is thus clear that C_1 represents the cross-correlation between the intensity timeseries of VCSEL1 $I_1(t)$ and time-delayed VCSEL2 $I_2(t\text{-}\tau)$. In contrast, C_2 means the cross-correlation between the intensity timeseries of VCSEL2 $I_2(t)$ and time-delayed VCSEL1 $I_1(t\text{-}\tau)$. By comparing C_1 and C_2, ones can determine the role of VCSEL1 and VCSEL2 in leader-lagged relationship: when $C_1 > C_2$, the VCSEL1 is the leader oscillating in advance of VCSEL2. On the contrary, the VCSEL2 will be the leader when $C_2 > C_1$.

3. Results

3.1. Basic characteristics of polarization chaos from free-running VCSELs

The *P-I* characteristics of the free-running VCSEL is analyzed in order to ensure its XP and YP outputs be chaotic at the same time. As shown in Fig. 2(a), the black and red line correspond to the *P-I* curve of the XP and YP output power from a free-running VCSEL with a normalized injection current μ varying from 1 to 3, respectively. The other simulation parameters can be seen in Table 1. From Fig. 2(a), we can observe that at the beginning ($1 < \mu < 1.3$), only the XP mode oscillates and the YP mode is suppressed. With increasing μ to 1.3, the YP mode starts to oscillate. Moreover, the XP and YP mode outputs coexist in the range of $1.3 < \mu < 3$. Figures 2(b) and 2(c) illustrate the associated bifurcation plot of the XP and YP outputs as a function of the normalized injection current μ. As μ increases, the VCSEL experiences a transition from periodic regime into chaotic state. Further observation can find that in the range of $1.5 < \mu < 2$, both the output of the XP and YP modes are chaotic.

Based on the above, we set the normalized injection current μ to be around 1.7 in the following simulations on chaos synchronization. Accurately, the injected currents μ_1 for VCSEL1 is set to 1.73, while the injected current μ_2 of VCSEL2 is 1.71. Figure 3 plots the associated intensity timeseries and self-correlation curves of their own chaotic outputs, respectively. From the timeseries [Figs. 3(a-1) and 3(b-1)], we can observe that the polarization chaos exhibits random fluctuation with large amplitudes. Moreover, we can confirm from Figs. 3(a-2) and 3(b-2) that there is indeed no so-called weak periodicity in polarization chaos due to the absence of external perturbations.

3.2. Polarization chaos synchronization by parallel optical injection

In this subsection, we investigate the LLCS in the scenario of parallel optical injection. Figure 4 maps the calculated difference value $\Delta C = C_2 - C_1$ in the parameter space of frequency detuning
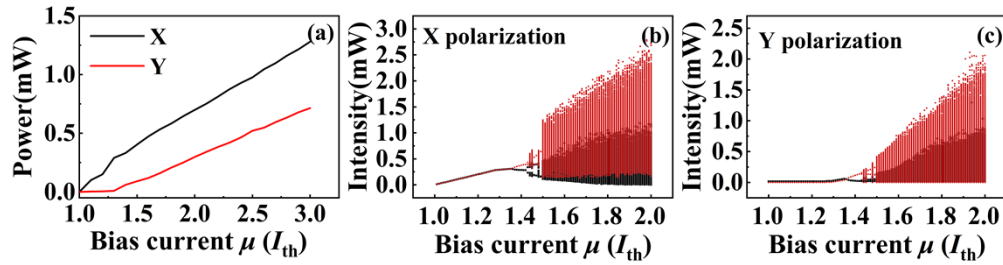
Fig. 2. (a) Average output intensity of XP mode (black line) and YP mode (red line) as a function of normalized injection current μ; (b) Bifurcation diagram of XP output versus the normalized injection current μ; (c) Bifurcation diagram of YP output versus the normalized injection current μ. In (b) and (c), the red dots and the black dots are top and bottom extrema of the associated chaotic timeseries, respectively.
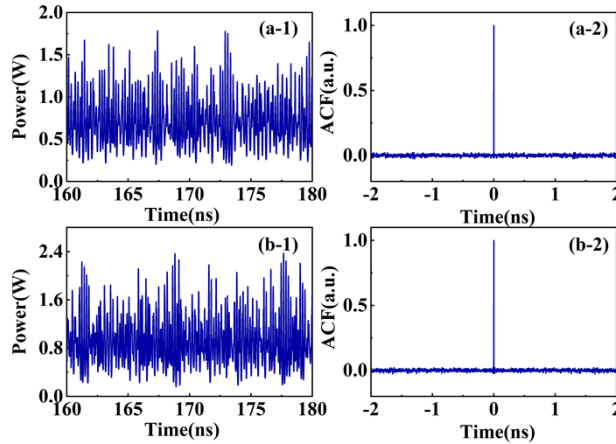

Fig. 3. (a-1) Time series and (a-2) self-correlation curve of the polarization chaos with a normalized bias current $\mu = 1.73$; (b-1) Time series and (b-2) self-correlation of the polarization chaos with a normalized bias current $\mu = 1.71$.

Δf and injection rate difference Δk_{inj} for the XP mode [Fig. 4(a)] and YP mode [Fig. 4(b)], respectively. As mentioned in Sec. II, the difference value ΔC can identify the leader-laggard relationship: $\Delta C > 0$ (green region) means the VCSEL2 is the leader, whilst $\Delta C < 0$ (red region) indicates the VCSEL1 is the leader; when ΔC is equivalent to 0, corresponding to the black dashed line in Fig. 4, an exchange in the leader-laggard relationship occurs between the VCSEL1 and VCSEL2. From Fig. 4, we can find that as Δf increases, the role of VCSEL1 changes from the original leader (red region) to the lagger (green region), no matter for the case of XP mode or YP mode.

We point that the injection locking is the origin why the exchange of the leader-laggard relationship occurs, which can be identified from the optical spectra [18]. Taking point A ($\Delta k_{\mathrm{inj}} = 0\,\mathrm{ns}^{-1}$, $\Delta f = 2\,\mathrm{GHz}$) in Fig. 4(a) as an representative, we investigate the role of the injection locking on the exchange of the leader-laggard relationship. Figure 5 shows the simulated optical spectra before and after the exchange of the leader-laggard relationship when the coupling is unidirectional. In this simulation, the optical spectra are obtained assuming that VCSEL1 is the leader before the exchange of the leader-laggard relationship. For clarity, we shift all the spectra of VCSEL2 downward with respect to the spectrum of VCSEL1. As shown in Fig. 5(a), when the light from VCSEL1 is injected to VCSEL2, the injection locking occurs. The evidence
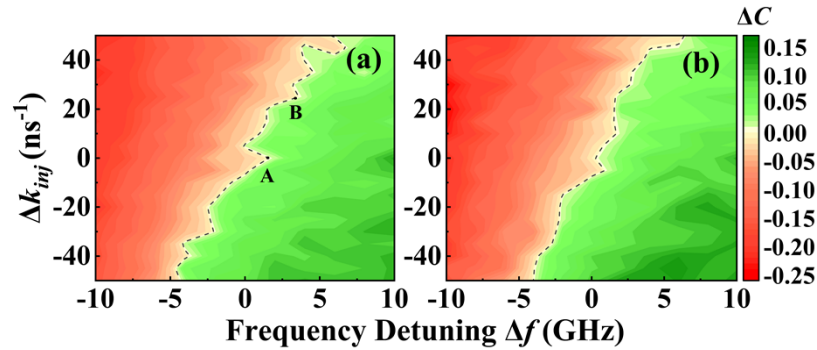
Fig. 4. Maps of $\Delta C = C_2 - C_1$ in the parameter space of Δf and Δk_{inj} for parallel optical injection. (a) XP mode and (b) YP mode.

is that VCSEL1 and VCSEL2 have their main peaks at the same frequency. In comparison, when the coupling is set from VCSEL2 to VCSEL1, the injection locking is not established as shown in Fig. 5(b): the dominant peak in VCSEL1 is no longer present, and its whole spectrum shows multiple separated peaks. This means that the injection locking synchronization between the two VCSELs will undergo a transition from injection locking of VCSEL1 by VCSEL2 to injection locking of VCSEL2 by VCSEL1.
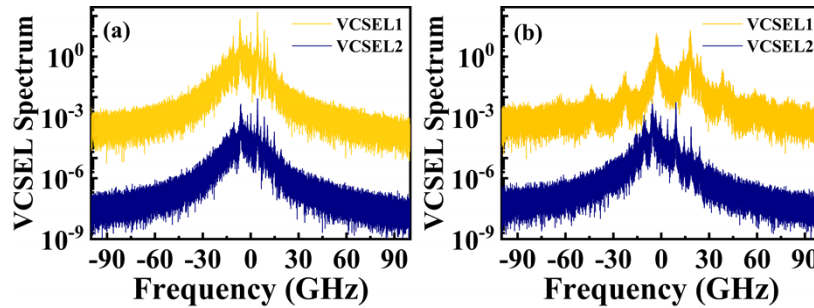
Fig. 5. Numerical optical spectra of VCSEL1 (yellow) and VCSEL2 (blue): (a) coupling from VCSEL1 to VCSEL2, and (b) coupling from VCSEL2 to VCSEL1. Injection locking is achieved in (a), but not in (b).

Furthermore, we find that around the dash line where the leader-laggard relationship exchanges, both the outputs of VCSEL1 and VCSEL2 usually exhibit the low frequency fluctuation (LFF) dynamics that consists of high-frequency chaotic oscillation and low-frequency intensity dropout [36,37]. Let us take point B ($\Delta k_{inj} = 24$ ns^{-1}, $\Delta f = 3$ GHz) in Fig. 4(a) for an example, where the injection strength is asymmetric ($k_{inj}^{1,2} \neq k_{inj}^{2,1}$). Keeping the same Δk_{inj} as that in point B, we change the frequency detuning Δf and then obtained the associated temporal waveforms before and after the leader-laggard transition as shown in Fig. 6. At the frequency detuning $\Delta f = 2.5$ GHz, it can be seen from Fig. 6(a) that VCSEL1 exhibits an intensity dropout earlier than VCSEL2 when VCSEL1 is the leader. When the frequency detuning Δf is set to be 3.5 GHz, the leader-laggard relationship exchanges and thus VCSEL2 oscillates in advance of VCSEL1. From Fig. 6(a) or Fig. 6(b), it can be observed clearly that a series of sudden decreases (labelled as dropout) in the intensity appear at a certain interval and the intensity gradually recovers after each dropout. After calculation, we find that the time interval in the recovery process corresponds to the round-trip propagation time of light between the two VCSELs ($2\Delta\tau = 6$ ns). This phenomenon that the intensity dropout and the gradual recovery is viewed as a typical

evidence of LFF dynamics just like in Refs. [20,21]. From this point of view, we thus believe that the occurrence of the exchange between the leader and laggard is related to the LFF dynamics of the mutually coupled lasers.
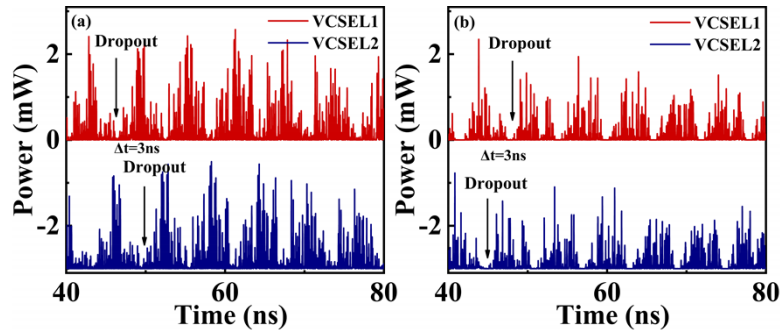
Fig. 6. (a) Temporal waveform of the laser intensity when VCSEL1 (red) is the leader; (b) Temporal waveform of the laser intensity when VCSEL2 (blue) is the leader.

At last, we consider the stability of the leader-laggard relationship. Generally, the leader-laggard relationship can be regarded to be stable when $|\Delta C| > 0.1$ [20]. In this condition, it can be found that both the XP and YP modes have a similar transformation trend: as the positive frequency detuning Δf increasing, the LLCS at the negative injection rate difference Δk_{inj} becomes more stable (green region) where the VCSEL2 is the leader; Conversely, in the region of negative frequency detuning Δf (red region), the LLCS at the positive injection rate difference Δk_{inj} is more stable with Δf decreasing, where the leader is the VCSEL2. In quantitative, the stable LLCS ($|\Delta C| > 0.1$) can be achieved in the region $5\,\text{GHz} < |\Delta f| < 10\,\text{GHz}$ with a relatively large parameter range of Δk_{inj}.

In addition, when the LLCS is stable, the outputs of VCSEL1 and VCSEL2 are completely developed chaos. Figure 7 shows a time series comparison, cross correlation function and synchronization diagram of the XP outputs from VCSEL1 and VCSEL2. In this simulation, $\Delta f = -10\,\text{GHz}$, $\Delta k_{inj} = 40\,\text{ns}^{-1}$ and the other parameter values are fixed as that mentioned before. From the chaotic temporal output by VCSEL1 and VCSEL2 in XP mode [Fig. 7(a)], we can see that the VCSEL1 is highly correlated with the delayed VCSEL2, and the VCSEL1 is the leader oscillating in advance by a propagation delay time $\tau = 3\,\text{ns}$. Note that the timeseries of VCSEL2 is shifted by -5 mW with respect to the timeseries of VCSEL1 for clarity. From Fig. 7(b), we can observe that here are two main peaks for $C_1 = 0.9536$ and $C_2 = 0.7111$, which induces ΔC can reach a maximum value of 0.242. Besides, we can also confirm that the chaotic outputs of VCSEL1 and VCSEL2 achieve stable leader-laggard relationship from their synchronization diagram in Fig. 7(c). The time series comparison, cross correlation function and synchronization diagram for the YP mode are similar with those in Fig. 7, so we do not give them for the sake of briefness.

### 3.3. Polarization chaos synchronization by orthogonal optical injection

In this subsection, we investigate the LLCS in the scenario of orthogonal optical injection. Figure 8 shows the ΔC function on the parameter space of Δf and Δk_{inj}. Figure 8(a) depicts the cross-correlation for XP mode of VCSEL1 with YP mode of VCSEL2, whereas Fig. 8(b) plots the cross-correlation for the YP mode of VCSEL1 with XP mode of VCSEL2. No matter in Figs. 8(a) or 8(b), the role of VCSEL1 changes from the leader to the laggard as the Δf increases (from the red region to green region) when Δk_{inj} is fixed. The dash lines correspond to a series of critical points where the exchange of the leader-laggard relationship. We confirm the reason why the leader-laggard role exchanges between VCSEL1 and VCSEL2 is the injection locking, which
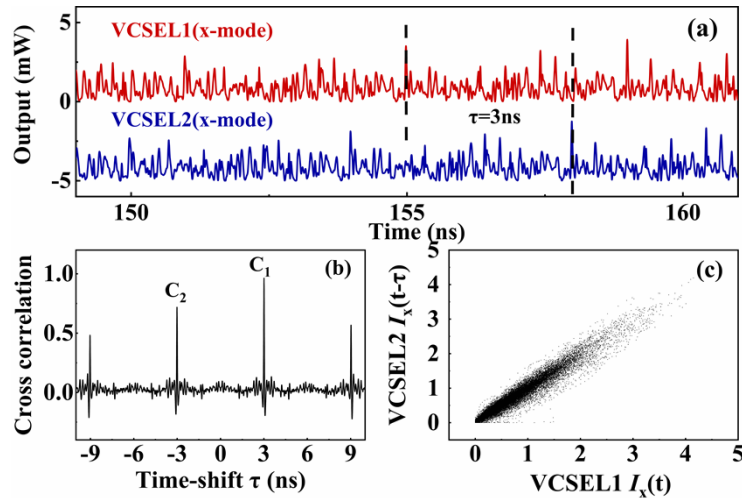
Fig. 7. (a) Time series of VCSEL1 (red) and VCSEL2 (blue) for the XP mode output; (b) Cross correlation function and (c) Synchronization diagram between the two XP output time series, where the timing of VCSEL2 is shifted in time -τ.

is the same as the case of parallel injection. For the sake of briefness, we do not give associated discussions like that in Figs. 5 and 6.
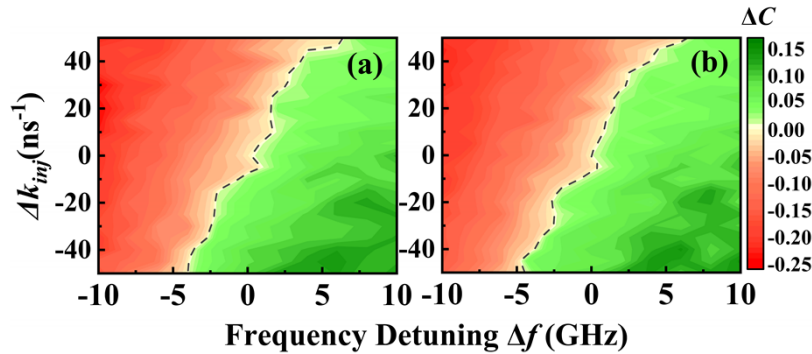
Fig. 8. Maps of $\Delta C = C_2 - C_1$ in the parameter space of Δf and Δk_{inj} for orthogonal optical injection. (a) XP of VCSEL1 versus YP of VCSEL2; (b) YP of VCSEL1 versus XP of VCSEL2.

About the stability of the leader-laggard relationship in the case of orthogonal optical injection there is the same feature as that in the case of parallel injection. In the upper left region (red region), VCSEL1 also acts as the leader. Moreover, the LLCS relationship becomes more stable with the decrease of Δf and the increase of Δk_{inj}. In the lower right corner (green region), VCSEL2 will be the leader, where the LLCS relationship becomes more stable with Δf increasing and Δk_{inj} decreasing. The whole stable region of LLCS for orthogonal optical injection is analogous with that in the case of parallel injection. But there is also a difference between them: the stability of orthogonal injection is higher than that in the case of parallel coupling at the same lower right region (green region) encircled by $3\,\text{GHz} < \Delta f < 10\,\text{GHz}$ and $-50\,\text{ns}^{-1} < \Delta k_{\text{inj}} < -10\,\text{ns}^{-1}$. For instance, when $\Delta f = 6\,\text{GHz}$ and $\Delta k_{\text{inj}} = -40\,\text{ns}^{-1}$, ΔC in Fig. 8(a) is 0.146, but 0.128 in Fig. 4(a).

Figure 9 shows the typical time series comparison, cross correlation function and synchronization diagram between the XP mode of VCSEL1 and the YP mode of VCSEL2 in the case of orthogonal injection at this parameter point ($\Delta f = 6$ GHz, $\Delta k_{inj} = -40$ ns^{-1}). From Fig. 9(a), we can see that VCSEL2 (the leader) oscillates in advance of VCSEL1 for the propagation delay time τ. Note, the timeseries of VCSEL2 is shifted downward by -6 mW with respect to the timeseries of VCSEL1 in Fig. 9(a). From Fig. 9(b), we can obtain that the two peaks are $C_1 = 0.7833$ and $C_2 = 0.9296$, respectively, where ΔC can reach a large value of 0.146. The linearity exhibits in the synchronization diagram between the timeseries of XP output of VCSEL1 and YP output of the VCSEL2 in Fig. 9(c) further confirm the establishment of a stable LLCS.
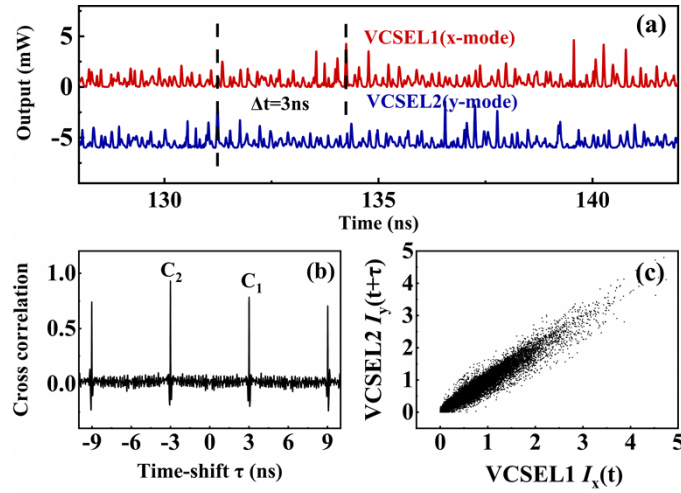

Fig. 9. (a) Time series of VCSEL1 (red) for the XP mode output and VCSEL2 (blue) for the YP mode output; (b) Cross correlation function and (c) Synchronization diagram between the timeseries of XP output of VCSEL1 and YP output of the VCSEL2, where the timing of VCSEL2 is shifted in time τ.

4. Discussions

In this section, we want to firstly discuss the impact of the parameter mismatch. Specifically, we quantitatively calculate C_1 and C_2 as a function of internal parameter mismatch. In this simulation, the internal parameters of VCSEL1 are fixed, and only the internal parameters of VCSEL2 are changed. Once there is a cross point between C_1 and C_2, an exchange in the leader-laggard relationship between the VCSEL1 and VCSEL2 occurs. Figure 10 illustrates some typical results about the effect of internal parameter mismatch on the exchange of the leader-laggard role. In the cases of parallel injection [Figs. (a1-f1)], Δk_{inj} is equivalent to be 0 while Δf is set to be 3 GHz. On the other hand, $\Delta k_{inj} = 0$ and $\Delta f = 0$ GHz is for the cases of orthogonal injection [Figs. (a2-f2)]. It can be observed from all the curves of C_1 and C_2 that a cross point appears for both parallel or orthogonal injection, but the cross points only exist in a relatively small mismatch range between -15% and 15%.

Then, we point that there are two possible methods for polarization chaos generation in practice. One is to use a kind of specially designed quantum dot (QD) VCSELs, called as 'submonolayer QD VCSELs' [38]. In this kind of VCSEL, the quantum dot active region is grown using a submonolayer technique (That is, without wetting layer and with lateral compositional modulation due to strain distribution when depositing several InAs submonolayers in a GaAs matrix). As experimentally demonstrated in Ref. [28], this VCSEL commonly emits two elliptically polarized modes with the increase of the bias current. Under an appropriate bias current, polarization
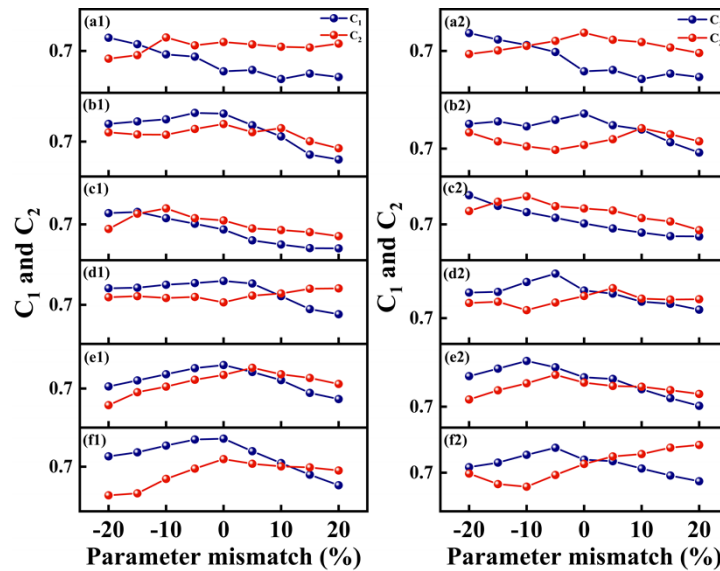
Fig. 10. Impact of the internal parameter mismatch on the leader-laggard relationship where C_1 (blue) and C_2 (red) are plotted as a function of mismatched (a) k, (b) α, (c) γ_a, (d) γ_N, (e) γ_s and (f) γ_p. The left column is for the cases of parallel injection, when the right column corresponds to the cases of orthogonal injection.

chaos appears due to the nonlinear coupling between the two lasing polarization modes. The other method can be achieved by means of a commercially available quantum well (QW) VCSEL under in-plane anisotropic mechanical strain. The anisotropic stress applied onto the QW gain medium can induce polarization dependent variations of its gain and refractive index. This in turn influences the nonlinear polarization dynamics of the QW VCSEL. When an appropriate strain level is applied, chaotic polarization fluctuations can also be observed using off-the-shelf QW VCSELs [39].

5. Conclusion

In sum, we have numerically demonstrated the leader-laggard relationship of polarization chaos synchronization in mutually coupled VCSELs with time delay. Specifically, the polarization chaos synchronization is observed in two scenarios: parallel injection and orthogonal injection. Through analyzing the difference of cross-correlation values, we find that the frequency detuning Δf is the dominant factor effecting the leader-lagged relationship compared with injection strength. Further investigation confirms the exchange between the leader and the laggard is induced by the injection locking from the origin. Final results show that there is a similar leader-laggard relationship in both cases of the parallel and orthogonal injection: stable LLCS forms in the two regions of (-10 GHz $< \Delta f <$ -5 GHz, -50 ns$^{-1} < \Delta k_{inj} <$ -10 ns^{-1}) and (5 GHz $< \Delta f <$ 10 GHz and, 10 ns$^{-1} < \Delta k_{inj} <$ 50 ns^{-1}) The maximum ΔC can reach 0.242 when the frequency detuning is negative, but only is 0.146 at a positive frequency detuning.

Disclosures. The authors declare no conflicts of interest.

References

1. P. Colet and R. Roy, "Digital communication with synchronized chaotic lasers," Opt. Lett. **19**(24), 2056–2058 (1994).
2. T. U. Singh, A. Nandi, and R. Ramaswamy, "Scenarios for generalized synchronization with chaotic driving," Phys. Rev. E **78**(2), 025205 (2008).
3. G. D. VanWiggeren and R. Roy, "Communications with chaotic lasers," Science **279**(5354), 1198–1200 (1998).
4. E. Klein, R. Mislovaty, I. Kanter, and W. Kinzel, "Public-channel cryptography using chaos synchronization," Phys. Rev. E **72**(1), 016214 (2005).
5. R. Vicente, C. R. Mirasso, and I. Fischer, "Simultaneous bidirectional message transmission in a chaos-based communication scheme," Opt. Lett. **32**(4), 403–405 (2007).
6. E. Klein, N. Gross, E. Kopelowitz, M. Rosenbluh, L. Khaykovich, W. Kinzel, and I. Kanter, "Public-channel cryptography based on mutual chaos pass filters," Phys. Rev. E **74**(4), 046201 (2006).
7. L. Keuninckx, M. C. Soriano, I. Fischer, C. R. Mirasso, R. M. Nguimdo, and G. Van der Sande, "Encryption key distribution via chaos synchronization," Sci. Rep. **7**(1), 43428 (2017).
8. F. Böhm, S. Sahakian, A. Dooms, G. Verschaffelt, and G. Van der Sande, "Stable High-Speed Encryption Key Distribution via Synchronization of Chaotic Optoelectronic Oscillators," Phys. Rev. Appl. **13**(6), 064014 (2020).
9. Y. Huang, P. Zhou, and N. Li, "High-speed secure key distribution based on chaos synchronization in optically pumped QD spin-polarized VCSELs," Opt. Express **29**(13), 19675–19689 (2021).
10. V. Flunkert, O. D'Huys, J. Danckaert, I. Fischer, and E. Scholl, "Bubbling in delay-coupled lasers," Phys. Rev. E **79**(6), 065201 (2009).
11. J. M. Buldu, T. Heil, I. Fischer, M. C. Torrent, and J. Garcia-Ojalvo, "Episodic synchronization via dynamic injection," Phys. Rev. Lett. **96**(2), 024102 (2006).
12. J. Mork and B. Tromborg, "Chaos in semiconductor lasers with optical feedback: theory and experiment," IEEE J. Quantum Electron. **28**(1), 93–108 (1992).
13. M. G. Rosenblum, A. S. Pikovsky, and J. Kurths, "From Phase to Lag Synchronization in Coupled Chaotic Oscillators," Phys. Rev. Lett. **78**(22), 4193–4196 (1997).
14. I. Fischer, G. V. Tartwijk, A. M. Levine, W. Elser, E. G. Bel, and D. Lenstra, "Fast pulsing and chaotic itinerancy with a drift in the coherence collapse of semiconductor lasers," Phys. Rev. Lett. **76**(2), 220–223 (1996).
15. W. L. Zhang, W. Pan, B. Luo, X. H. Zou, M. Y. Wang, and Z. Zhou, "Chaos synchronization communication using extremely unsymmetrical bidirectional injections," Opt. Lett. **33**(3), 237–239 (2008).
16. P. Rees, P. S. Spencer, I. Pierce, S. Sivaprakasam, and K. A. Shore, "Anticipated chaos in a nonsymmetric coupled external-cavity-laser system," Phys. Rev. A **68**(3), 033818 (2003).
17. T. Heil, I. Fischer, W. Elsässer, J. Mulet, and C. R. Mirasso, "Chaos synchronization and spontaneous symmetry-breaking in symmetrically delay-coupled semiconductor lasers," Phys. Rev. Lett. **86**(5), 795–798 (2001).
18. M. Ozaki, H. Someya, T. Mihara, A. Uchida, S. Y. oshimori, K. Panajotov, and M. Sciamanna, "Leader-laggard relationship of chaos synchronization in mutually coupled vertical-cavity surface-emitting lasers with time delay," Phys. Rev. E **79**(2), 026210 (2009).
19. N. Jiang, W. Pan, B. Luo, L. Yan, S. Xiang, L. Yang, D. Zheng, and N. Li, "Properties of leader-laggard chaos synchronization in mutually coupled external-cavity semiconductor lasers," Phys. Rev. E **81**(6), 066217 (2010).
20. K. Kanno, T. Hida, A. Uchida, and M. Bunsen, "Spontaneous exchange of leader-laggard relationship in mutually coupled synchronized semiconductor lasers," Phys. Rev. E **95**(5), 052212 (2017).
21. T. Mihana, Y. Mitsui, M. Takabayashi, K. Kanno, S. Sunada, M. Naruse, and A. Uchida, "Decision making for the multi-armed bandit problem using lag synchronization of chaos in mutually coupled semiconductor lasers," Opt. Express **27**(19), 26989 (2019).
22. C. M. González, M. C. Torrent, and J. García-Ojalvo, "Controlling the leader-laggard dynamics in delay-synchronized lasers," Chaos **17**(3), 033122 (2007).
23. J. Ohtsubo, "*Semiconductor Lasers: Stability, Instability and Chaos*," (Springer, 2007).
24. D. Rontani, E. Mercier, D. Wolfersberger, and M. Sciamanna, "Enhanced complexity of optical chaos in a laser diode with phase-conjugate feedback," Opt. Lett. **41**(20), 4637–4640 (2016).
25. W. L. Zhang, W. Pan, B. Luo, M. Y. Wang, and X. H. Zou, "Synchronization performance comparison of vertical-cavity surface-emitting lasers with two different feedback chaos schemes," Semicond. Sci. Technol. **20**(9), 979–984 (2005).
26. D. Rontani, A. Locquet, M. Sciamanna, D. S. Citrin, and S. Ortin, "Time-delay identification in a chaotic semiconductor laser with optical feedback: A dynamical point of view," IEEE J. Quantum Electron. **45**(7), 879–1891 (2009).
27. M. C. Soriano, J. García-Ojalvo, C. R. Mirasso, and I. Fischer, "Complex photonics: Dynamics and applications of delay-coupled semiconductors lasers," Rev. Mod. Phys. **85**(1), 421–470 (2013).
28. M. Virte, K. Panajotov, H. Thienpont, and M. Sciamanna, "Deterministic polarization chaos from a laser diode," Nat. Photonics **7**(1), 60–65 (2013).
29. P. H. Mu, W. Pan, and N. Q. Li, "Analysis and characterization of chaos generated by free-running and optically injected VCSELs," Opt. Express **26**(12), 15642–15655 (2018).
30. M. Virte, M. Sciamanna, and K. Panajotov, "Synchronization of polarization chaos from a free-running VCSEL," Opt. Lett. **41**(19), 4492–4495 (2016).
31. Z. R. Wang, P. Li, Z. W. Jia, W. Wang, B. J. Xu, K. A. Shore, and Y. Wang, "Synchronization of polarization chaos in mutually coupled free-running VCSELs," Opt. Express **29**(12), 17940–17950 (2021).

32. M. Virte and F. Ferranti, "Chaos in Solitary VCSELs: Exploring the Parameter Space with Advanced Sampling," J. Lightwave Technol. **36**(9), 1601–1607 (2018).

33. M. Virte and F. Ferranti, "Chaos-Preserving Reduction of the Spin-Flip Model for VCSELs: Failure of the Adiabatic Elimination of the Spin-Population Difference," IEEE J. Sel. Top. Quantum Electron. **25**(6), 1–8 (2019).

34. J. M. Regalado, F. Prati, M. S. Miguel, and N. B. Abraham, "Polarization Properties of Vertical-Cavity Surface Emitting Lasers," IEEE J. Quantum Electron. **33**(5), 765–783 (1997).

35. P. Pérez, A. Valle, and L. Pesquera, "Polarization-resolved characterization of long-wavelength vertical-cavity surface-emitting laser parameters," J. Opt. Soc. Am. B **31**(11), 2574–2580 (2014).

36. W. Ray, G. Lam, and R. Roy, "Observation of chaotic itinerancy in the light and carrier dynamics of a semiconductor laser with optical feedback," Phys. Rev. E **73**(2), 026219 (2006).

37. T. Sano, "Antimode dynamics and chaotic itinerancy in the coherence collapse of semiconductor lasers with optical feedback," Phys. Rev. A **50**(3), 2719–2726 (1994).

38. F. Hopfer, A. Mutig, M. Kuntz, G. Fiol, D. Bimberg, N. N. Ledentsov, V. A. Shchukin, S. S. Mikhrin, D. L. Livshits, and I. L. Krestnikov, "Single-mode submonolayer quantum-dot vertical-cavity surface-emitting lasers with high modulation bandwidth," Appl. Phys. Lett. **89**(14), 141106 (2006).

39. T. R. Raddo, K. Panajotov, B. H. V. Borges, and M. Virte, "Strain induced polarization chaos in a solitary VCSEL," Sci. Rep. **7**(1), 14032 (2017).